DOI: 10.1002/chem.200501329

Nanocrystalline Lanthanide Nitride Materials Synthesised by Thermal Treatment of Amido and Ammine Metallocenes: X-ray Studies and DFT Calculations

Ulrich Baisch,[a] Sandro Pagano,[a] Martin Zeuner,[a] Noémi Barros,[b] Laurent Maron,[b] and Wolfgang Schnick*[a]

Abstract: The decomposition process of ammine lanthanide metallocenes was studied by X-ray diffractometry, spectroscopy and theoretical investigations. A series of ammine-tris(η^5-cyclopentadienyl)lanthanide(III) complexes **1**-Ln (Lanthanide (Ln) = Sm, Gd, Dy, Ho, Er, Yb) was synthesised by the reaction of [Cp_3Ln] complexes (Cp = cyclopentadienyl) with liquid ammonia at −78 °C and structurally characterised by X-ray diffraction methods, mass spectrometry and vibrational (IR, Raman) spectroscopy. Furthermore, amido-bis(η^5-cyclopentadienyl)lanthanide(III) complexes **2**-Ln (Ln = Dy, Ho, Er, Yb) were synthesised by heating the respective ammine adduct **1**-Ln in an inert gas atmosphere at temperatures of between 240 and 290 °C. X-ray diffraction studies, mass spectrometry and vibrational (IR, Raman) spectroscopy were carried out for several **2**-Ln species and proved the formation of dimeric μ_2-bridged compounds. Species **1**-Ln are highly reactive coordination compounds and showed different behaviour regarding the decomposition to **2**-Ln. The reaction of **1**-Ln and **2**-Ln with inorganic bases yielded lanthanide nitride LnN powders with an estimated crystallite size of between 40 and 90 nm at unprecedented low temperatures of 240 to 300 °C. Temperature-dependent X-ray powder diffraction and transmission electron microscopy (TEM) investigations were performed and showed that the decomposition reaction yielded nanocrystalline material. Structural optimisations were carried out for **1**-Ln and **2**-Ln by employing density functional (DFT) calculations. A good agreement was found between the observed and calculated structural parameters. Also, Gibbs free energies were calculated for **1**-Ln, **2**-Ln and the pyrolysis reaction to the nitride material, and were found to fit well with the expected ranges.

Keywords: density functional calculations · lanthanide nitrides · ligands · metallocenes · molecular precursors

Introduction

Recently, a broad variety of novel lanthanide-containing materials has been investigated, giving rise to promising applications. Although oxidic rare-earth materials are still dominant,[1–7] nitridic rare-earth compounds are gaining more and more importance as they often exhibit even better material properties. Advances in the fields of semi- and superconductivity,[8–10] heterogeneous and homogeneous catalysis,[11–13] and the development of novel phosphor materials for highly efficient white-light-emitting phosphor-converted diodes[14,15] are prominent examples that prove that nitride chemistry of the rare-earth elements is full of exciting reactions and useful applications.

New pathways to simple nitrogen-containing compounds are of general interest, especially in solid-state chemistry, in which basic compounds are often obtained in a higher purity by non-classical reaction routes. Binary lanthanide nitrides are amongst fundamental rare-earth materials. There are, however, only a few synthetic approaches known for the synthesis of such simple compounds with defined composition. Molecular precursor compounds, such as [Ln{N($SiMe_3$)$_2$}$_3$],[16] or the reaction of rare-earth chlorides with lithium nitride,[17,18] emerged as alternative procedures for

[a] U. Baisch, S. Pagano, M. Zeuner, Prof. Dr. W. Schnick
Ludwig-Maximilians-Universität München
Department Chemie und Biochemie
Butenandtstraße 5–13 (D), 81377 München (Germany)
Fax: (+49) 89-2180-77440)
E-mail: wsc@cup.uni-muenchen.de

[b] N. Barros, Dr. L. Maron
Laboratoire de Physique Quantique, IRSAMC, UMR 5626 (CNRS)
Université Paul Sabatier, 118, route de Narbonne
31062 Toulouse cedex 4 (France)

the synthesis of LnN at temperatures of less than 500 °C. These approaches have been studied for both thin-film deposition and bulk solid syntheses of metal nitrides.[17] With respect to their importance for several applications in solid-state rare-earth chemistry, a facile synthetic method to produce reactive lanthanide nitride powders at low temperatures (below 300 °C) is desirable.

As we are generally targeting new nitride-containing materials employing molecular-precursor syntheses,[19–26] we have recently started to utilise organolanthanide molecular precursors for the synthesis of highly activated rare-earth nitrido compounds.

Organolanthanide complexes have been used frequently in the field of catalysis,[12,13,27–29] however, they also represent highly reactive species for the synthesis of novel functionalised materials.[3]

Therefore, we searched for a simple molecular precursor with ligands showing an adequate thermal lability for subsequent pyrolysis reactions. Nitrogen should be already present in the complex in order to achieve preorganisation at the metal centre. Nevertheless, other ligands or fragments should be easily removable during the decomposition process.

In the 1960s, Wilkinson[30] and Fischer[30–33] synthesised the first rare-earth metallocenes and observed their ability to bind ammonia. Further investigations on the ytterbium compound revealed that ammine-tris(η^5-cyclopentadienyl)-ytterbium(III) [Cp_3YbNH_3] (**1**-Yb; Cp = cyclopentadienyl) can be isolated easily by sublimation in vacuo.[31,32,34] Subsequent heating under normal pressure yielded bis-[amido-bis(η^5-cyclopentadienyl)ytterbium(III)] [{Cp_2YbNH_2}$_2$] [**2**-Yb; Eq. (1) and (2)].[31–35]

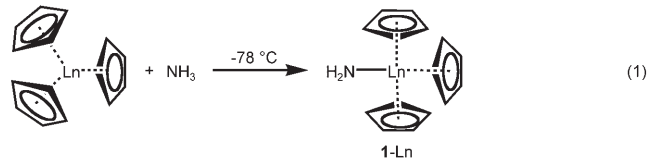

(1)

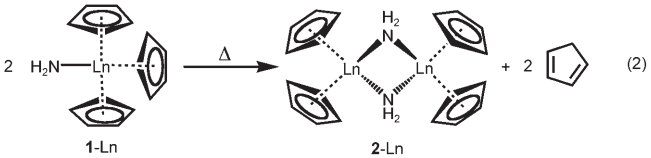

(2)

These complexes show thermal stability up to almost 400 °C and a high reactivity towards acids and bases. The high stability of the ammonia ligand demonstrates the strong interaction of nitrogen with the metal centre and proves that this system might be appropriate for our purposes.

Analytical data were available especially for the Yb compound.[31,33–36] Thus, first and foremost we had to focus on the synthesis of [Cp_3Ln] ammoniates and amides of other rare-earth elements (Sm, Gd, Dy, Ho, Er). The existence of neither [Cp_3LnNH_3] nor [{Cp_2LnNH_2}$_2$] has been confirmed previously by crystal-structure determinations. The knowledge of the arrangement of the complex molecules in the unit cell gave us the possibility to consider also packing effects for their solid-state reactivity. Therefore, we report here the first crystal-structure determinations of [Cp_3GdNH_3] (**1**-Gd), [Cp_3DyNH_3] (**1**-Dy), [Cp_3HoNH_3] (**1**-Ho), [Cp_3ErNH_3] (**1**-Er), [Cp_3DyNH_3] (**2**-Dy), [{Cp_2HoNH_2}$_2$] (**2**-Ho), [{Cp_2ErNH_2}$_2$] (**2**-Er) and [{Cp_2YbNH_2}$_2$] (**2**-Yb).

To the best of our knowledge, the next step, a solid-state decomposition reaction of either **1**-Ln or **2**-Ln to nitride compounds, has not yet been described in the literature. The pyrolysis of these reactive complexes in the presence of inorganic bases yielded LnN in most satisfying quality, reactivity and at very low temperatures.

Based on the experimentally postulated reaction mechanism, DFT calculations were carried out on the amido and ammine complexes and for the reaction to the nitride compounds. Calculations on lanthanide complexes are of increasing interest, but are still rather scarce in the literature. The 4f electrons do not participate in the chemical bonding,[37] which allowed the use of relativistic effective core potentials (RECPs)[38–40] including these electrons into the core (not treated explicitly). Moreover, DFT (B3PW91)[41,42] calculations on lanthanide complexes were successfully performed on a wide variety of reaction mechanisms involving lanthanide centres.[43–46] The lanthanide centres were treated with the previously described large-core RECPs together with their adapted basis sets. All other atoms (carbon, hydrogen or nitrogen) were treated with an all-electron double-ζ basis set augmented by a set of polarisation function (p for hydrogen and d for carbon and nitrogen). All the structures were optimised without symmetry constraints by using the Gaussian 98 suite of programs.[47] The natures of the minima were verified by analytic determination of vibrational frequency. The optimised geometry can be compared directly to the refinement results of the X-ray data, because the experimental complexes involved real Cp (C_5H_5) rings and no ligand modelling was necessary. This comparison will be useful for checking the validity of the theoretical approach. Due to the complexity of the reaction mechanism involving phase changes, only thermodynamic data of the reactions in the gas phase at room temperature and at 300 °C were computed. Furthermore, as it was shown previously that calculated reaction energies are not very sensitive to the change of lanthanide centre[44] (energy change of 1–2 kcal mol^{-1}), reaction energies at 300 °C were computed for selected lanthanides only (Dy and Sm).

Results and Discussion

Ammine-tris(η^5-cyclopentadienyl) lanthanides (1-Sm, 1-Gd, 1-Dy, 1-Ho, 1-Er): Cp_3 complexes of lanthanides show a high affinity for the coordination of NH_3. All these complexes (Ln = Pr, Nd, Sm, Eu, Gd, Dy, Ho, Er, Yb) are re-

ported to decolourise upon stirring in liquid ammonia.[30,32] However, the true composition of the products formed is still unknown. The formation of large NH-bridged complexes (oligomers) seems probable, in which more than one NH_3 molecule can be involved in the coordination sphere of the central atom.

After evaporating and pumping off residual NH_3, most of the compounds become coloured again and form ammoniates. The stability of the isolated species towards sublimation varies significantly for the different lanthanide metals: The ammonia adducts of [Cp_3Yb], [Cp_3Er], [Cp_3Ho] and [Cp_3Gd] are easily formed and were obtained with satisfying purity and yields. In contrast, those of [Cp_3Dy] and [Cp_3Sm] showed only moderate yields after sublimation, and [Cp_3Ce], [Cp_3Eu] and [Cp_3Nd] did not form sublimable ammine complexes, even after prolonged stirring in liquid ammonia. Actually, [Cp_3Ce], [Cp_3Nd] and [Cp_3Eu] decolourise upon stirring in NH_3, but after evaporation of the liquid, the original colour reappeared again and the starting compounds were recovered. In contrast, the Yb, Er, Ho, Gd, Dy and Sm compounds obtained showed a remarkable thermal stability up to 300 °C.

To understand this variation of reactivity towards ammonia in the solid state, we performed a more detailed investigation of these complexes. As only partial analytical data was available for the ammonia adducts of the known lanthanide–Cp_3 complexes (elemental analysis for Pr,[30] Sm,[30] nothing for Eu,[30] for Yb only:[30,31,33,48] elemental analysis, IR/NIR/UV/Vis), we also characterised the synthesised compounds by using IR/Raman spectroscopy, mass spectrometry and single-crystal X-ray diffraction analysis.

*Spectroscopic measurements for **1**-Ln*: Each of the obtained ammonia adducts of the lanthanide–Cp_3 complexes (**1**-Sm, **1**-Eu, **1**-Gd, **1**-Dy, **1**-Ho, **1**-Er, **1**-Yb) was characterised by IR and Raman spectroscopy. The coordinated ammonia can be identified easily by the strong N–H stretching vibrations at around 3365, 3330 and 3250 cm^{-1} and by the intense asymmetrical and symmetrical N–H deformation modes at around 1600, 1225 and 500 cm^{-1} seen in the infrared spectra of **1**-Sm, **1**-Gd, **1**-Dy, **1**-Ho, **1**-Er and **1**-Yb (Figure 1). The vibrations differ only slightly, within a range of ± 7 cm^{-1}, from one complex to the other. Complexes **1**-Sm and **1**-Gd show additional shoulders in these regions. The seven typical stretching ($2\,\nu_{(CH)}$, $2\,\nu_{(CC)}$) and deformation ($1\,\delta_{(CH)}$ parallel, $2\,\delta_{(CH)}$ perpendicular) vibrations of the cyclopentadienyl rings at 3090, 3070, 1440, 1360, 1010, 790 and 775 cm^{-1} were also observed and differ only slightly from one complex to the other.[30,31] Only very weak NH-absorption signals were found for the Nd and Eu compounds. Therefore, there was no convincing evidence for the formation of significant amounts of either **1**-Nd or **1**-Eu.

The Raman spectra correspond well with the IR results, but show only weak intensities for the N–H vibrations (Figure 1 for **1**-Er). The most intense signal at 1130 cm^{-1} can be attributed to a symmetrical expansion of the Cp rings. The strong signals of less than 400 cm^{-1} correspond to the expected signal-rich spectrum for a metal centre surrounded by three Cp ligands in a trigonal pyramidal manner (metal-ring deformation and stretching modes for the molecular skeleton).

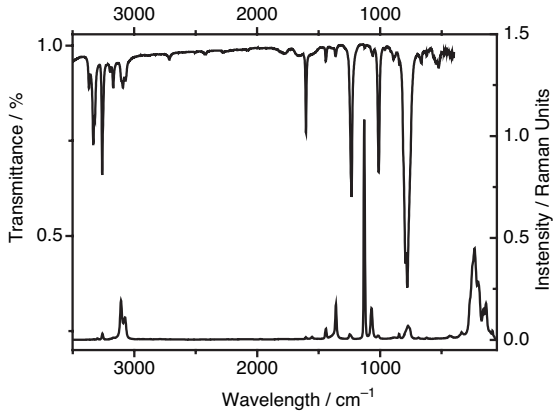

Figure 1. Raman (right, bottom) and IR (left, top) spectra of [Cp_3ErNH_3] (**1**-Er).

Mass spectrometry data for **1**-Dy were collected and exhibit the typical defragmentation pattern for metallocene complexes. Sequential loss of C_5H_5 ($m/z = 65$) occurred, forming [Cp_3Ln^+], [Cp_2Ln^+] and [$CpLn^+$], respectively. The most intense peak corresponds to the $C_5H_5^+$ fragment. The [M^+] peak of the compound was not observed, due to the severe conditions of the EI (electron ionisation) experiment. Once ionised, the NH_3 ligand seems to detach immediately. Therefore, measurements for lower m/z were carried out and clearly showed the presence of free NH_3 at $m/z = 17$.

Structural data: The complexes **1**-Gd, **1**-Dy, **1**-Ho and **1**-Er were definitively characterised by X-ray crystallography. Accordingly, all were found to consist of mononuclear species, however, these complexes are not isostructural as they do not crystallise in the same space group. Table 1 shows that **1**-Gd crystallises in a cubic primitive lattice exhibiting a higher symmetric molecular structure than **1**-Dy, **1**-Ho and **1**-Er, which crystallise in a monoclinic primitive space group. Figure 2 shows the molecular structure of **1**-Er. Comparative crystallographic data for all of the characterised compounds are given in Table 1, and bond lengths and angles are listed in Table 2 (Ln–Ctr = distance between the centre of the C_5-plane (centroid) and the central atom).

The distances between the Cp rings and the lanthanide atoms correspond well to the expected ranges given in the literature for the solvated Cp_3 complexes. Figure 3 shows the variation of the metal–ligand distances as a function of the atomic number of the respective lanthanides.

The Ln–Cp distances decrease slightly as atomic number increases, due to the lanthanide contraction. The Cp–Ln distances vary slightly (within 2 pm) for **1**-Dy, **1**-Ho and **1**-Er. This effect was observed and discussed for several metallocenes with three or four Cp ligands and is normally based on attraction by the ligands of neighbouring complexes in

Table 1. Crystallographic data for the $[Cp_3LnNH_3]$ complexes **1**-Gd, **1**-Dy, **1**-Ho and **1**-Er.

	1-Gd	**1**-Dy	**1**-Ho	**1**-Er
formula	$C_{15}H_{18}NGd$	$C_{15}H_{18}NDy$	$C_{15}H_{18}NHo$	$C_{15}H_{18}NEr$
M_r	369.55	374.80	377.23	379.56
T [K]	130	130	150	130
size [mm^3]	0.12x0.11x0.11	0.10x0.05x0.04	0.13x0.12x0.10	0.20x0.14x0.06
crystal system	cubic	monoclinic	monoclinic	monoclinic
space group	$Pa\bar{3}$	$P2_1/c$	$P2_1/c$	$P2_1/c$
a [pm]	1411.5(2)	825.9(2)	826.8(2)	823.0(2)
b [pm]	–	1102.1(2)	1103.8(2)	1099.1(2)
c [pm]	–	1481.6(3)	1482.0(3)	1477.2(3)
β [°]	–	101.61(3)	101.60(3)	101.57(3)
V [$\times 10^6$ pm^3]	2812.2(6)	1321.0(5)	1325.0(5)	1309.0(5)
Z	8	4	4	4
ρ_{calcd} [Mg m^{-3}]	1.746	1.885	1.891	1.926
F(000)	1432	724	728	732
μ [mm^{-1}]	4.695	5.633	5.948	6.388
refl. collected	22913	30071	12412	18375
independent refl.	1137	5801	2986	2984
no. of parameters	53	213	163	140
R(int)	0.0922	0.0792	0.0452	0.0676
$R1$ [$I>2\sigma(I)$]	0.0444	0.0374	0.0204	0.0302
$wR2$ (all data)	0.1301	0.0584	0.0395	0.0658
max. peak/min. hole [e Å^{-3}]	1.517/−1.032	1.371/−2.520	0.788/−0.640	1.780/−1.827

the structure.[31,49] In this type of compounds the attraction of the ammonia ligand seems to be a crucial structure-determining factor. Except for **1**-Gd, the Ln–N distances match the shortest M–Cp distances of the complexes exactly. Interestingly, the Cp ligand closest to the central atom also exhibits the closest contact to the NH_3 ligand of the neighbouring complex. Only in **1**-Gd does the Ln–N distance differ significantly from the Cp–Gd distances.

Until now, no explanation has been given as to why **1**-Sm and **1**-Gd do not undergo decomposition to the respective amido complexes at higher temperatures [Eq. (2)]. The structural observations made above, and the distances of Ln–N shown in Figure 3 for all of the complexes characterised, could give a reasonable explanation for this difference in the reactivity of **1**-Sm, **1**-Gd, **1**-Dy, **1**-Ho, **1**-Er and **1**-Yb towards pyrolysis to the amido derivatives. Due to its higher molecular symmetry, all the Cp–Ln distances in complex **1**-Gd are equal, but at the same time the distance Gd–N increases to almost 250 pm. The Gd–N and the Dy–N distances differ by about 6 pm.

Furthermore, there are no differences in the intermolecular distances to the neighbouring Cp ligands for $[Cp_3GdNH_3]$, in contrast to **1**-Dy, **1**-Ho and **1**-Er (see above). Thus, the neighbouring Cp ligands can no longer interact well with the coordinated ammonia in an intermolecular manner. Figure 4 shows these packing differences clearly for **1**-Ho and **1**-Gd. Presumably, these solid-state effects

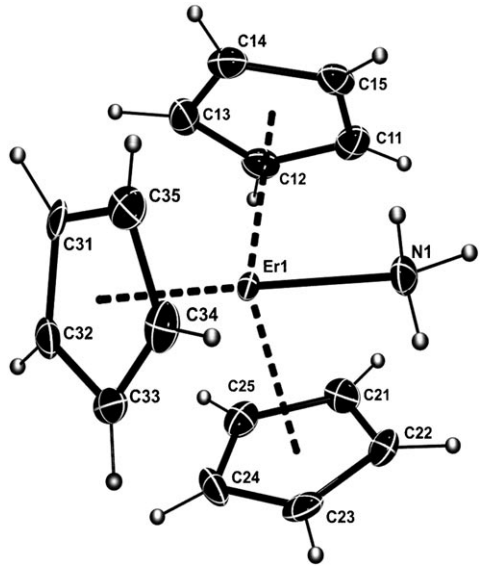

Figure 2. Molecular structure of $[Cp_3ErNH_3]$ (**1**-Er) at 130 K (50% probability ellipsoids). The hydrogen atoms were calculated (Cp rings) or unequivocally found in the difference Fourier map (ammine group), respectively, and refined with fixed isotropic thermal parameters.

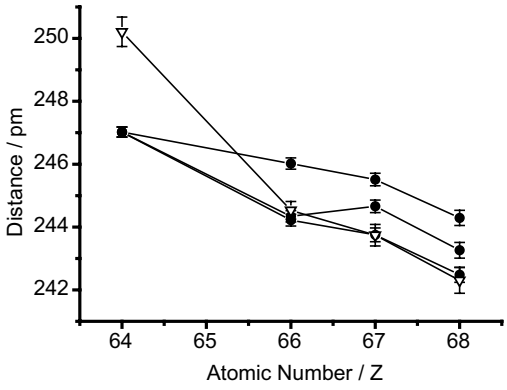

Figure 3. Metal–ligand distances (pm) as a function of the atomic number of the respective lanthanides of the ammine complexes of Gd(64), Dy(66), Ho(67), Er(68). ▽: Ln–N distances; ●: Ln–Cp distances; error bars are depicted for each value.

Table 2. Selected bond lengths [pm] and angles [°] for $[Cp_3LnNH_3]$ complexes **1**-Gd, **1**-Dy, **1**-Ho and **1**-Er.

Compound	**1**-Gd	**1**-Dy	**1**-Ho	**1**-Er
Ln–N	250.1(6)	244.5(3)	243.7(4)	242.3(5)
Ln–Ctr(1)	247.1(2)	244.2(2)	243.8(3)	242.5(3)
Ln–Ctr(2)	–	244.3(2)	244.7(2)	243.3(3)
Ln–Ctr(3)	–	246.0(2)	245.5(2)	244.3(3)
N-Ln-Ctr(1)	101.0(2)	97.22(2)	97.19(2)	97.28(3)
N-Ln-Ctr(2)	–	98.35(2)	98.56(2)	98.41(3)
N-Ln-Ctr(3)	–	99.01(2)	99.01(2)	99.07(3)
Ctr(1)-Ln-Ctr(2)	116.6(2)	117.89(2)	117.83(2)	117.93(3)
Ctr(1)-Ln-Ctr(3)	–	118.04(2)	118.01(2)	117.93(3)
Ctr(2)-Ln-Ctr(3)	–	118.08(2)	118.08(2)	118.06(3)

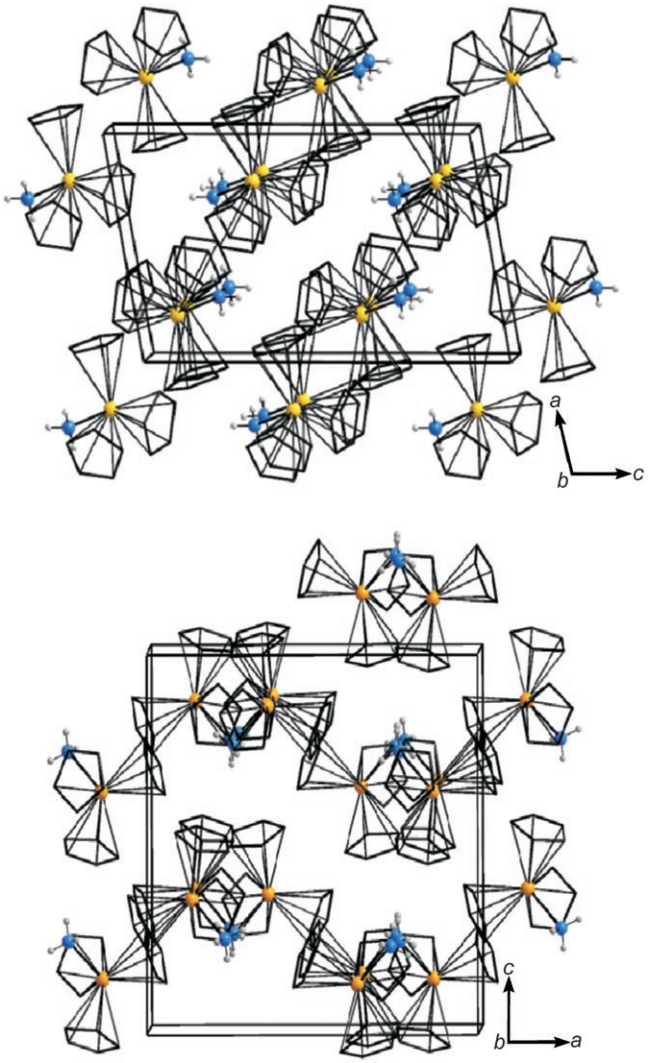

Figure 4. Projection of the unit cell of **1**-Ho (top) and **1**-Gd (bottom) on the *ac* plane.

could be responsible for the absence of decomposition leading to $[\{Cp_2GdNH_2\}_2]$ and $[\{Cp_2SmNH_2\}_2]$.

DFT calculations for $[Cp_3LnNH_3]$: Geometry optimisations were carried out for **1**-Sm, **1**-Gd, **1**-Dy, **1**-Ho and **1**-Er. The characteristic geometrical parameters are presented in Table 3.

The optimised bond lengths, either Ln–Cp or Ln–N, are in good agreement with the experimental values. The maximum deviation is obtained for the Dy–N bond, which is overestimated by 9 pm. Notably, all the calculated bond lengths are slightly larger than the experimental ones, but remain within the range of the admitted precision of calculations (10 pm). Moreover, the experimental trend (decrease of the bond lengths as atomic number increases) is reproduced by the calculation. This decrease is apparently associated with the lanthanide contraction, as mentioned before. It has been reported that the lanthanide contraction is correctly reproduced by DFT calculations (B3PW91). Contrary to experimental results, for all lanthanide complexes, the Ln–N distance is found to be slightly longer than the Ln–Cp distance (3–6 pm), and the **1**-Gd complex does not exhibit any special behaviour. However, the observed discrepancy between Ln–N and Ln–Cp distances is lower than the common accuracy of the theoretical method used. The calculated bond angles are also found to be in agreement with the X-ray data (maximum deviation of 3° for Gd).

The Gibbs free energies of bonding of NH_3 to $[Cp_3Ln]$ complexes were calculated at two different temperatures (25 and 300 °C) and are presented in Table 4. These bonding energies were obtained by considering the Gibbs free energies of the complex with the two relaxed fragments.

Table 4. Bonding Gibbs free energies [kcal mol^{-1}] in $[Cp_3LnNH_3]$ complexes **1**-Sm, **1**-Gd, **1**-Dy, **1**-Ho and **1**-Er.

	25 °C	300 °C		25 °C	300 °C
Sm	−7.12	2.55	Gd	−6.97	–
Dy	−6.57	3.25	Ho	−6.43	–
Er	−6.30	–			

Notably, the reactions are found to be exergonic at room temperature for all lanthanides, but slightly endergonic at 300 °C. This can be explained simply by the fact that the reaction is under entropy control, as there is a loss of translational entropy between free ammonia and coordinated ammine. The stability (up to 280 °C) is fairly well reproduced by the calculations as, at 300 °C, the reactions are only slightly endergonic. The calculated bonding energy is found to decrease along the series and this is in agreement with an increase of steric repulsion between the Cp rings.

Amido-bis(η^5-cyclopentadienyl) lanthanides (2-Dy, 2-Ho, 2-Er, 2-Yb): Amido–Cp_2 complexes of erbium and ytterbium have been discussed in the literature and can also be prepared by using other synthetic approaches (**2**-Er, **2**-Yb).[34,50] However, difficulties in synthesising further $[\{Cp_2LnNH_2\}_2]$ species with different lanthanides have been reported.[31,50]

Table 3. Selected bond lengths [pm] and angles [°] for $[Cp_3LnNH_3]$ complexes **1**-Sm, **1**-Gd, **1**-Dy, **1**-Ho and **1**-Er.

$[Cp_3LnNH_3]$	Ln–Cp^1	Ln–Cp^2	Ln–Cp^3	Cp^1-Ln-Cp^2	Cp^1-Ln-Cp^3	Cp^2-Ln-Cp^3	Ln–N	N-Ln-Cp^1	N-Ln-Cp^2	N-Ln-Cp^3
$[Cp_3SmNH_3]$	254	254	254	118.7	118.7	118.6	260	96.7	97.0	96.6
$[Cp_3GdNH_3]$	252	252	252	118.6	118.6	118.6	256	97.0	96.7	96.7
$[Cp_3DyNH_3]$	249	249	249	118.6	118.6	118.6	253	96.7	96.7	97.0
$[Cp_3HoNH_3]$	247	249	250	118.6	118.4	118.7	252	96.9	96.9	97.0
$[Cp_3ErNH_3]$	247	247	247	118.7	118.6	118.6	250	96.7	97.0	96.7

Furthermore, to the best of our knowledge, no crystal-structure investigations have been reported for **2**-Ln.

The decomposition of **1**-Er, **1**-Ho and **1**-Dy according to Equation (2) yielded **2**-Er, **2**-Ho and **2**-Dy, respectively. These compounds exhibit a remarkable thermal stability. The products show melting points of greater than 300 °C (determined by differential scanning calorimetry (DSC) measurements). On the other hand, **2**-Dy, **2**-Ho and **2**-Er are highly reactive towards acids and other bases. The difficulty in decomposing $[Cp_3LnNH_3]$ to $[\{Cp_2LnNH_2\}_2]$ increases as the atomic number of the lanthanide element decreases. Thus, it has not yet been possible to obtain **2**-Gd and **2**-Sm. In the same sequence of the lanthanides, the yields of the reactions from $[Cp_3LnNH_3]$ to $[\{Cp_2LnNH_2\}_2]$ significantly decrease from **2**-Yb to **2**-Dy.

Spectroscopic measurements: Complexes **2**-Dy, **2**-Ho, **2**-Er and **2**-Yb were characterised by IR and Raman spectroscopy. The μ_2-briged amido ligand can be identified easily by the intense N–H stretching vibrations at 3350, 3290 cm^{-1} and the intense asymmetrical and symmetrical N–H deformation modes at around 1540, 670 and 440 cm^{-1}. A strong vibration mode at 3500 cm^{-1}, probably due to a combination of two lower signals, is typical for each of the synthesised amido compounds (Figure 5). The modes differed from one

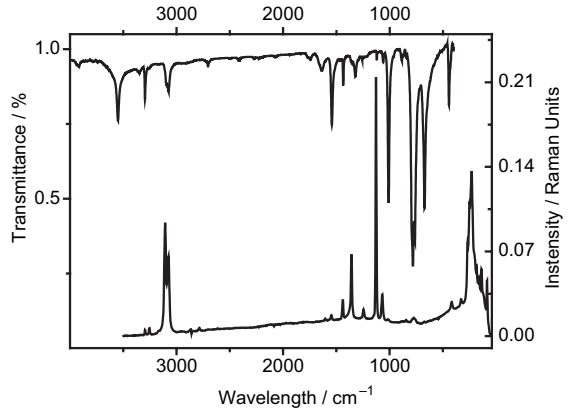

Figure 5. Raman (right, bottom) and IR (left, top) spectra of $[\{Cp_2HoNH_2\}_2]$ (**2**-Ho).

metal ion to the other significantly and lay within a range of ± 20 cm^{-1}, which is greater than for the respective ammoniates. Also, the seven typical stretching (2 $\nu_{(CH)}$, 2 $\nu_{(CC)}$) and deformation (1 $\delta_{(CH)}$ parallel, 2 $\delta_{(CH)}$ perpendicular) vibrations for the cyclopentadienyl rings at 3080, 3070, 1435, 1360, 1010, 790 and 775 cm^{-1}, respectively, were identified and differ only slightly for the different complexes.

Raman measurements correspond well with the IR spectroscopy results, but show only weak intensities for the N–H vibrations. Figure 5 shows this fact clearly for **2**-Ho. The most intense signal at 1130 cm^{-1} can be attributed to a symmetrical expansion of the Cp rings. The strong signals of less than 400 cm^{-1} represent the expected signal-rich spectrum for a metallocene compound with additional ligands. These signals can be attributed to metal-ring deformation and stretching modes for the molecular skeleton. The stretching vibration for the Ln–NH_2 bond is represented by a very weak signal at 850 cm^{-1}.

Mass spectrometry data for **2**-Dy and **2**-Ho were collected and showed a defragmentation pattern similar to that published for **2**-Yb.[35,36] Sequential loss of C_5H_5 ($m/z = 65$) and decomposition of NH_2 was observed, forming $[Cp_3Ln_2N_2H_4^+]$, $[Cp_3Ln_2NH^+]$, $[Cp_2Ln_2N_2H_4^+]$, $[Cp_2Ln_2NH^+]$, $[Cp_2Ln_2^+]$, $[Cp_3Ln^+]$, $[Cp_2Ln^+]$, $[CpLn^+]$ and Ln^+. The most intense peak in the spectrum changed for the different compounds. Compounds **2**-Dy and **2**-Yb exhibit their most intense peak at $m/z = 552$ ($[Cp_3Ln_2N_2H_4^+]$) and $m/z = 294$ ($[Cp_2Ln^+]$). For **2**-Ho, the most intense peak was centred at $m/z = 66$ and represents the $C_5H_6^+$ fragment. Also, the intensity of the $[M^+]$ signals changed significantly. Compounds **2**-Dy and **2**-Yb showed intensities at the 15 % level, whereas the $[M^+]$ signal of **2**-Ho showed a relative height of 3 %.

Structural data: Single crystals were obtained for **2**-Dy, **2**-Ho, **2**-Er and **2**-Yb and were characterised by X-ray crystallography. All four complexes are dimeric, but exhibit different packing of the molecules in the solid, and different space groups exist. Compound **2**-Er crystallises in the highly symmetric space group $Im\bar{3}$, in contrast to **2**-Dy, **2**-Ho and **2**-Yb, for which the monoclinic space group $P2_1/n$ was observed (Table 5).Changes in types of structure and crystal symmetry due to variation of the lanthanide ion are quite common. However, in the series **2**-Dy, **2**-Ho, **2**-Er and **2**-Yb the cubic erbium compound seems to be an exception to the rule, as the neighbouring lanthanides on both the right and left sides form isotypic monoclinic amido lanthanide metallocene complexes. As already suggested from the mass-spectrometric investigations, the amido complexes are dimeric with two μ_2-bridged amido ligands (Figure 6). Compound **2**-Er shows a crystal structure with a remarkably high symmetry. The four Cp rings are oriented to each other in an eclipsed position, so that only three of the five carbon atoms are situated in the asymmetrical unit (Figure 7). Comparative crystallographic data for all of the characterised compounds are given in Table 5, and bond lengths and angles are listed in Table 6.

The distances between the Cp rings and the metal atoms in **2**-Dy and **2**-Yb (calculated as the distances between the centre of the C_5-plane (Ctr) and the central atom) are smaller than those in the respective ammine complexes. The formation of dimeric lanthanocene species with μ_2-briged ligand atoms is well known for the chloro-bis(cyclopentadienyl) lanthanides.[51–54] These compounds were considered as reference structures for the discussion of intramolecular distances obtained for the **2**-Ln complexes. Although the Ln–Cp distances of **2**-Dy and **2**-Yb are up to 5 pm longer than those of the chloro species, the angles Cp-Ln-Cp are quite similar. They coincide quite precisely at values between 129 and 130°. The angles Ln-N-Ln vary only slightly, by less than 2°, from those of $[\{Cp_2LnCl\}_2]$. Figure 8 shows

Table 5. Crystallographic data for the [{Cp_2LnNH_2}$_2$] complexes **2**-Dy, **2**-Ho, **2**-Er and **2**-Yb.

	2-Dy	**2**-Ho	**2**-Er	**2**-Yb
formula	$C_{20}H_{24}N_2Dy_2$	$C_{20}H_{24}N_2Ho_2$	$C_{20}H_{24}N_2Er_2$	$C_{20}H_{24}N_2Yb_2$
M_r	617.42	622.27	626.94	638.49
T [K]	150	150	130	150
crystal system	monoclinic	monoclinic	cubic	monoclinic
size [mm^3]	0.09x0.08x0.06	0.11x0.09x0.06	0.22x0.18x0.16	0.17x0.16x0.15
space group	$P2_1/n$	$P2_1/n$	$Im\bar{3}$	$P2_1/n$
a [pm]	842.4(2)	843.2(2)	1435.1(2)	848.9(2)
b [pm]	1065.6(2)	1064.6(2)	–	1057.5(2)
c [pm]	1123.2(2)	1119.3(2)	–	1113.7(2)
β [°]	106.86(3)	107.07(3)	–	107.72(3)
V [$\times 10^6$ pm^3]	964.9(4)	960.5(3)	2955.6(6)	952.4(4)
Z	2	2	6	2
ρ_{calcd} [Mg m^{-3}]	2.125	2.152	2.113	2.224
F(000)	580	584	1764	596
μ [mm^{-1}]	7.686	8.180	8.462	9.761
refl. collected	8072	8649	21358	1720
independent refl.	2295	2290	638	1720
no. of parameters	131	154	44	110
R(int)	0.0395	0.0529	0.0547	0.0517
$R1$ [$I > 2\sigma(I)$]	0.0210	0.0258	0.0258	0.0417
$wR2$ (all data)	0.0403	0.0552	0.0526	0.1121
max. peak/min. hole [e Å^{-3}]	0.918/−0.566	1.057/−0.618	0.698/−0.656	1.930/−1.867

The two crystallographically independent distances from the Cp ligands to the central atom vary only slightly, however, the values for the contacts Ln–N are remarkably different for **2**-Dy, **2**-Ho and in particular for **2**-Yb (Figure 8). In contrast to the measurements at room temperature, this effect increases at low temperatures. The analogous chloro complexes did not show this behaviour.[51–54] Due to the high crystal symmetry, the Ln–N distances in **2**-Er are equivalent.

The two nitrogen and metal atoms of the dimeric complex form a rhombus in **2**-Er and a parallelogram in **2**-Dy, **2**-Ho and **2**-Yb. For the earlier lanthanides the formation of infinite double chains could be possible, as reported for chloro-bis(cyclopentadienyl)-dysprosium(III).[51] However, to the best of our knowledge, attempts to synthesise [{Cp_2LnNH_2}$_2$], with Gd or any earlier lanthanide, have not yet been successful.

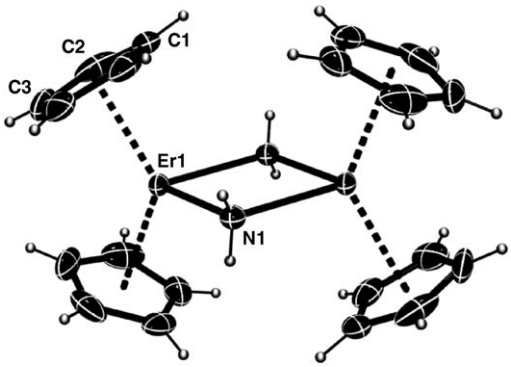

Figure 6. Molecular structure of [{Cp_2ErNH_2}$_2$] (**2**-Er) at 130 K (50% probability ellipsoids). The positions of all hydrogen atoms were unequivocally located in the difference Fourier map and refined with fixed isotropic thermal parameters.

Table 6. Selected bond lengths [pm] and angles [°] for [{Cp_2LnNH_2}$_2$] complexes **2**-Dy, **2**-Ho, **2**-Er and **2**-Yb.

Compound	**2**-Dy	**2**-Ho	**2**-Er	**2**-Yb
Ln–N	235.3(4)	233.8(6)	232.5(2)	229(1)
Ln–N*	236.8(4)	234.7(6)	–	233(1)
Ln–Ctr1	240.2(3)	238.5(3)	236.0(2)	234.6(7)
Ln–Ctr2	240.3(3)	237.9(4)	236.0(2)	234.3(6)
Ctr1-Ln-Ctr2	129.7(3)	129.7(3)	130.8(1)	130.2(7)
N-Ln-Ctr1	106.8	107.1	108.5	107.4
N*-Ln-Ctr1	109.6	109.7	–	109.2
N-Ln-Ctr2	108.3	108.5	108.5	108.3
N*-Ln-Ctr2	111.1	110.8	–	110.7
N-Ln-N*	79.5(2)	79.6(2)	80.8(1)	80.2(4)
Ln-N-Ln*	100.5(2)	100.4(2)	99.2(1)	99.8(4)
Ctr1-Ln-Ln-Ctr2	4.4	3.9	0.0	3.0

the variation of the distances between the metal atoms and the ligands as a function of the atomic numbers of the lanthanides **2**-Dy and **2**-Yb.

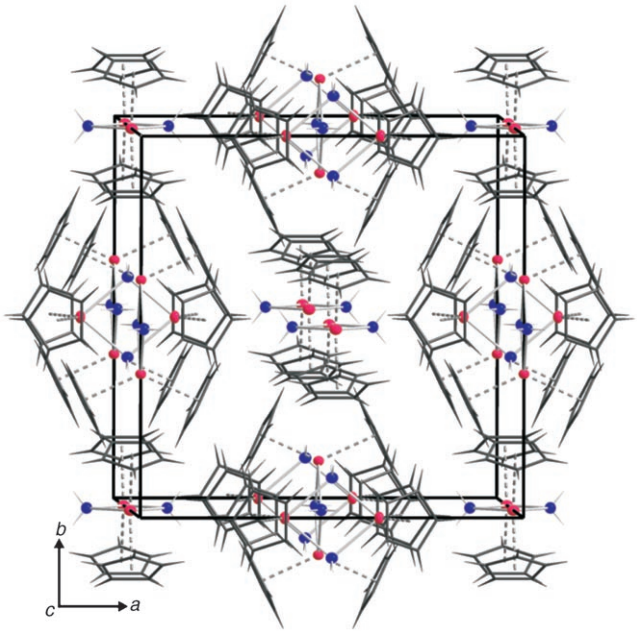

Figure 7. Projection of the unit cell of [{Cp_2ErNH_2}$_2$] (**2**-Er) on the *ab* plane.

Thermal treatment of the ammine complexes causes a loss of one hydrogen atom of the ammonia group and formation of the respective dimeric amido complexes. Although the NH group exhibits a higher Lewis basicity, a further deprotonation of the amido group could be possible. To

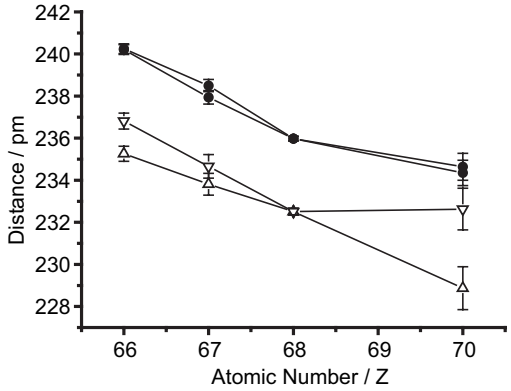

Figure 8. Bond lengths (pm) of the amido complexes of Dy(66), Ho(67), Er(68), Yb(70) as a function of the atomic number of the corresponding lanthanide. ▽ and △: Ln–N distances; ●: Ln–Cp distances; error bars are depicted for each value.

investigate the thermal behaviour of the amido lanthanide metallocene complexes, temperature-dependent X-ray powder diffraction (XRD) and differential scanning calorimetry (DSC) experiments of **2**-Ho and **2**-Yb were performed at temperatures of up to 700 °C.

A further dehydrogenation and the formation of nitrides was observed. The amido complexes **2**-Ho and **2**-Yb show melting points of between 320 and 360 °C and decompose to the nitrides at temperatures less than 400 °C. The temperature-dependent XRD measurements also shed light on the observation of different types of structure with different space groups for **2**-Er, **2**-Ho and **2**-Yb. These compounds undergo phase transitions at temperatures of between 220 and 300 °C to form higher symmetrical cubic phases. These are the same temperatures necessary to sublime this compound under vacuum. Nevertheless, until now we had not succeeded in obtaining suitable single crystals of monoclinic **2**-Er or cubic **2**-Ho.

DFT calculations for [{Cp_2LnNH_2}$_2$]: The computational cost/demands of DFT calculations increases rapidly as the number of atoms increases. Consequently, the dimers [{Cp_2LnNH_2}$_2$] were not studied explicitly. The geometry optimisations were, thus, performed for the monomers [Cp_2LnNH_2] of **2**-Er, **2**-Ho, **2**-Dy and **2**-Sm. The characteristic geometrical parameters are presented in Table 7. The dimerisation of the complex should affect the Cp–Ln bond lengths only slightly, so that a comparison between the theoretical and experimental Ln–Cp distances is relevant. In contrast, the Ln–N distances probably increase from the monomer to the dimer, so that the calculated distances should be underestimated with respect to the X-ray data.

Table 7. Selected bond lengths [pm] and angles [°] for [{Cp_2LnNH_2}$_2$] complexes **2**-Sm, **2**-Dy, **2**-Ho and **2**-Er.

[Cp_2LnNH_2]	Ln–N	Ln–Cp^1	Ln–Cp^2	N-Ln-Cp^1	N-Ln-Cp^2	Cp^1-Ln-Cp^2
[Cp_2SmNH_2]	223	249	249	110.8	110.9	138.3
[Cp_2DyNH_2]	217	241	241	111.2	111.3	137.5
[Cp_2HoNH_2]	216	241	241	111.2	111.3	137.4
[Cp_2ErNH_2]	215	238	239	111.2	111.2	137.6

Similarly to the calculations elaborated for **1**-Ln, the calculated Ln–Cp bond lengths for **2**-Ln are in good agreement with the X-ray data, with a maximum error of 3 pm for the Ho–Cp distances. The Ln–Cp distance still decreases from Sm to Er, due to the lanthanide contraction. These results confirm that the Ln–Cp bond lengths are not affected by dimerisation. However, the modelling of the dimers **2**-Ln by monomers has several effects. Firstly, the Ln–N distances are found to be smaller in the monomers than in the dimers by about 17 pm. Moreover, in the monomers, the calculated angles are larger than the experimental ones (about 8° for the Cp-Ln-Cp angles and 3–6° for the N-Ln-Cp angles). This can be understood by the fact that in the dimer, the steric repulsion between the Cp rings of each [Cp_2LnNH_2] moiety is enhanced. This repulsion should decrease the Cp-Ln-Cp angle of each moiety. In any case, the experimental trend from **1**-Ln to **2**-Ln is qualitatively reproduced: in the latter, the Ln–N bonds are shorter and the N-Ln-Cp angles are smaller.

As only the monomer was optimised, the thermodynamic data were computed for the reaction: [Cp_3LnNH_3]→[Cp_2LnNH_2]+CpH. The Gibbs free energy of this reaction was calculated at room temperature and at 300 °C (Table 8).

Table 8. Gibbs free energy of the decomposition [kcal mol^{-1}] to **2**-Sm, **2**-Dy, **2**-Ho and **2**-Er.

	25 °C	300 °C		25 °C	300 °C
Sm	21.58	5.83	Dy	17.03	1.60
Ho	15.80	–	Er	15.79	–

The decomposition reaction is calculated to be quite endergonic at room temperature and more favorable at high temperature. The calculated enthalpy of reaction is very high (about 31 kcal mol^{-1} at 25 °C) and stable with respect to the temperature (about 30 kcal mol^{-1} at 300 °C). Thus, the important difference in Gibbs free energies can be explained by the entropic effect. Indeed, the calculated entropic term is positive, because two molecules are released. Consequently, at high temperature, at which the effect of entropy is larger, the reaction becomes thermodynamically favorable. This can explain the high temperature that is required experimentally for this decomposition reaction. The highly positive reaction enthalpy might be explained by the loss of electronic delocalisation between the aromatic Cp ring in the lanthanide complex and the released C_5H_6. Moreover, the theoretical results could provide a qualitative explanation for why the decomposition of **1**-Sm to **2**-Sm could not be observed experimentally; this reaction was calculated to be about 4 kcal mol^{-1} more endergonic for **1**-Sm than **1**-Dy at 25 and 300 °C.

Pyrolysis to lanthanide nitrides: Because of the strong Ln–N bond, the dimeric amido complexes $[\{Cp_2LnNH_2\}_2]$ (**2**-Ln) decompose at temperatures greater than 400 °C to form the respective binary lanthanide nitrides. Large amounts of graphite are formed as a byproduct, because the Cp ligands start to carbonise at this temperature. To avoid the formation of carbon, nanocrystalline and purer nitride powders LnN, in which Ln = Sm, Gd, Dy, Ho, Er or Yb, were prepared by using solid-state metathesis reactions, according to Equations (3)–(5):

$$[Cp_2LnNH_2] + 2\,LiNH_2 \xrightarrow{\Delta T} LnN + 2\,LiCp + 2\,NH_3 \quad (3)$$

$$[Cp_3LnNH_3] + 3\,LiNH_2 \xrightarrow{\Delta T} LnN + 3\,LiCp + 3\,NH_3 \quad (4)$$

$$[Cp_2LnNH_2] + CaH_2 \xrightarrow{\Delta T} LnN + CaCp_2 + 2\,H_2 \quad (5)$$

Due to the basicity of the amido ligand, a strong base was necessary to achieve deprotonation of the coordinated amide. Both alkaline and alkaline-earth amides, as well as their hydrides, were used as reactants. Lithium amide and calcium hydride were found to be most appropriate for our purposes, because LiCp and $[Cp_2Ca]$, respectively, are formed as byproducts. These compounds can be easily removed from the reaction system by sublimation at temperatures greater than 200–250 °C in vacuo. Only traces of carbon remained in the product after evacuation and, thus, a brownish solid LnN was obtained after the pyrolysis.

Powder diffractometry and determination of crystal size: The formation of nitride material LnN was monitored by conducting temperature-dependent X-ray diffraction experiments. According to Equations (3)–(5), **2**-Dy, **2**-Ho, **2**-Er and **2**-Yb, and **1**-Sm, **1**-Gd, **1**-Ho, **1**-Er and **1**-Yb formed nitrides at temperatures of between 220 and 240 °C. The amido compounds seem to form purer products, evidenced by the formation of smaller amounts of graphite during the decomposition process. Elemental analysis of the products obtained showed graphite impurities of 1–3 and 2–5 % upon using **2**-Ln or **1**-Ln, respectively. Given the observation that not all lanthanides seem to form the amido compound easily, the synthesis of nitrides directly from the ammoniates represents an acceptable alternative. Figure 9 shows the XRD patterns obtained within a temperature range from room temperature up to 640 °C for the reaction of **2**-Er with $LiNH_2$, and an XRD pattern after annealing **2**-Dy with $LiNH_2$ at 400 °C. The formation of the byproduct LiCp confirms the reaction of $LiNH_2$ with **2**-Dy [Eq. (3) and (4)]. X-ray data of crystalline LiCp[55] was used to calculate a simulated XRD pattern of LiCp and was compared with the pattern of the crude reaction product (Figure 9, bottom).

Crystalline LnN can be recognised easily by the appearance of two broadened reflections at 14.5 and 16.8° ($\lambda_{Mo\text{-}K\alpha}$), which can be attributed to the (111) and (200) reflections, respectively. Whereas the LnN reflections start to grow significantly above 240 °C, the LiCp reflections (at 7.0, 7.6, 8.0, 10.8 and 11.5°, $\lambda_{Mo\text{-}K\alpha}$) are already present at 180 °C and remain until decomposition occurs at 500 °C. The early formation of this byproduct can be regarded as proof for the subsequent elimination of the Cp rings. $LiNH_2$ exhibits one characteristic reflection at 13.8° ($\lambda_{Mo\text{-}K\alpha}$), which rapidly looses intensity at between 220 and 320 °C as the binary nitride LnN is formed. The decomposition temperature for formation of the nitrides according to Equation (3) did not change for the different lanthanides (Dy, Ho, Er, Yb). Temperature-dependent XRD measurements of mixtures of the ammoniates **1**-Ln with $LiNH_2$ [Eq. (4)] showed that nitride powders can be obtained without preliminary synthesis of the amido compounds. Consequently, nanocrystalline SmN and GdN can be synthesised easily, starting directly from **1**-Sm or **1**-Gd, although synthesis of the amido derivative has so far been unsuccessful. Figure 10 shows XRD patterns (13–19°, $\lambda_{Mo\text{-}K\alpha}$) of the nitride material obtained from the pyrolysis reaction of **1**-Sm (a), **1**-Gd (b), **1**-Dy (c), **2**-Ho (d), **1**-Er (e), **2**-Er (f), **1**-Yb (g). Figure 10 shows clearly that differences in the crystallinity do not occur by using the ammine or the amido complex (e.g., patterns e and f). In contrast, the use of CaH_2, according to Equation (5), resulted in the formation of more crystalline HoN material (Figure 10d). Additionally, the powder pattern of the product shows clear-

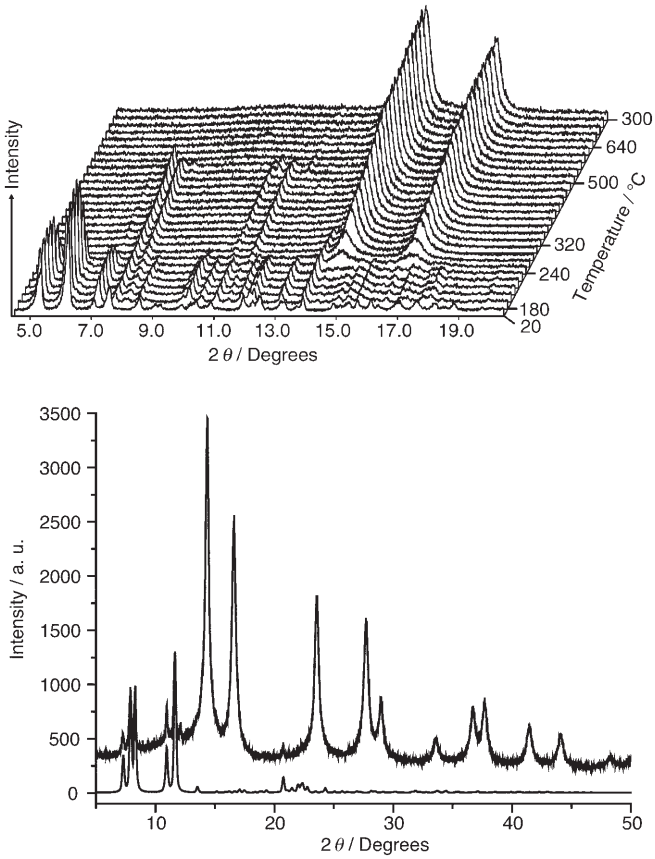

Figure 9. Top: temperature-dependent XRD patterns of the reaction of **2**-Er with $LiNH_2$ between 20 and 300 °C under Ar atmosphere ($\lambda_{Mo\text{-}K\alpha}$ = 0.71073 Å). Bottom: XRD pattern of the crude product of the reaction of **1**-Dy with $LiNH_2$ after annealing at 350 °C. The simulated XRD of LiCp is depicted at the bottom.

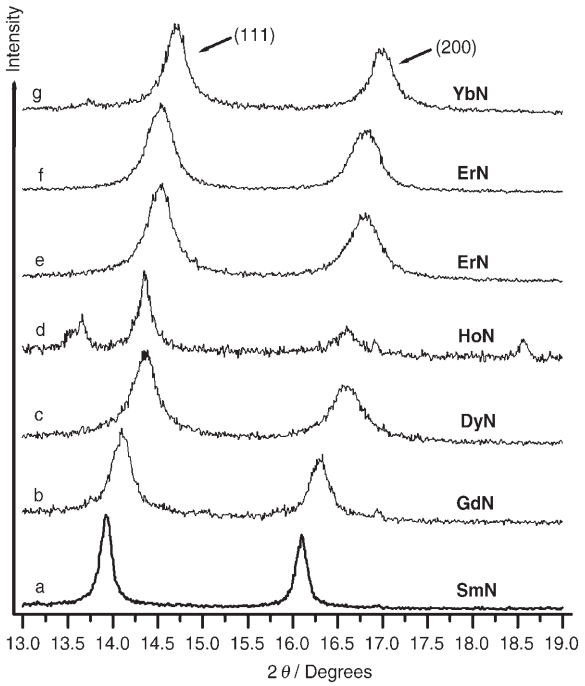

Figure 10. Diffraction patterns showing the most intense (111) and (200) reflections of LnN registered during temperature-dependent XRD measurements at 300 °C ($\lambda_{Mo\text{-}K\alpha}$ = 0.71073 Å). Precursors used: a) **1**-Gd + $LiNH_2$, b) **1**-Sm + $LiNH_2$, c) **1**-Dy + $LiNH_2$, d) **2**-Ho + $CaNH_2$, e) **1**-Er + $LiNH_2$, f) **2**-Er + $LiNH_2$, g) **1**-Yb + $LiNH_2$.

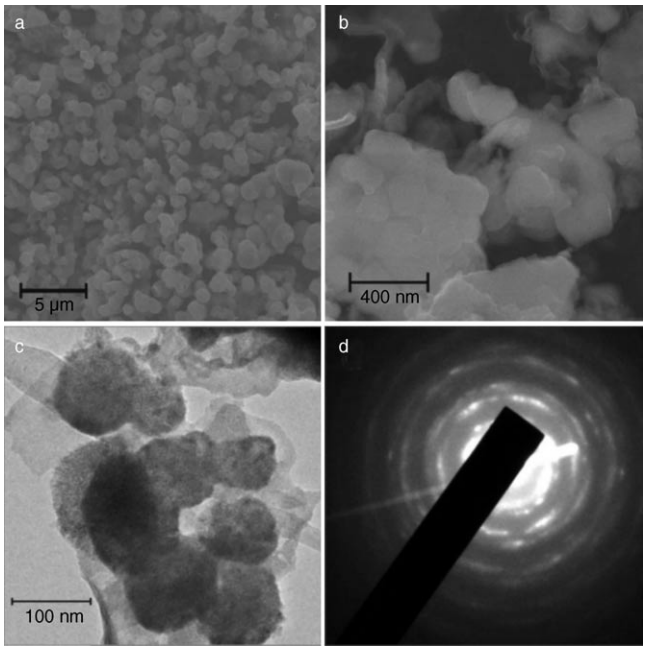

Figure 11. a) SEM image of ErN showing the bulky nitride powder. b) Enlarged SEM image of the ErN powder. c) TEM image of ErN crystallites. d) Corresponding ED pattern showing the ErN phase.

ly the presence of impurities identified as CaH_2 reflections at 13.5 and 18.6°.

According to the Scherrer equation, broadened reflections indicate that crystallites in the powder are smaller than approximately 100 000 unit cells of the substance. With a = 483.9 pm for the cubic structure of ErN, the particle sizes in a powder diffraction pattern with broadened reflections must be significantly smaller than 225 nm (edge length). From the Scherrer equation, based on the XRD line width, the ErN crystallite sizes should be within the range 10–40 nm. This value cannot be confirmed clearly by the results of scanning electron microscopy (SEM) experiments because of the formation of agglomerates. SEM images of the bulky material are depicted in Figure 11a,b.

Consequently, transmission electron microscopy (TEM) measurements were recorded. The crude product showed particle sizes of between 80 and 100 nm (Figure 11c). Electron diffraction (ED) experiments on these particles proved the crystallinity of the product and confirmed the formation of LnN (Figure 11d). Unfortunately, contamination with oxygen cannot be avoided during the preparation of the probe for the TEM measurement. Therefore, the quality of the crystallites was not as good as that obtained directly after the decomposition reaction. Agglomerated nanocrystals only were found during the TEM experiment, therefore, diffraction experiments on the polycrystalline material were elaborated.

From Figure 11d a very crude estimation for some lattice distances could be made. Powder patterns calculated subsequently were in good agreement with the literature 2θ values for crystalline ErN powder. Thus, the X-ray diffraction experiments of the LnN powder and the electron microscopy measurements agreed well with each other and proved the formation of nanocrystalline nitride material.

Calculations for the pyrolysis reactions: Because the experiment involved solid compounds and phase transitions, the calculated Gibbs free energy of reaction in the gas phase will certainly not be in agreement with the experimental observations. However, some qualitative information could be extracted from these calculations. Thus, Gibbs free energies for Equations (3) and (4) were computed at 25 and 300 °C (Table 9). As expected, the Gibbs free energies decreasing as the temperature decreases, which can be explained by entropic considerations. However, for both temperatures and a given lanthanide, the two reactions are calculated to be highly endergonic. This is qualitatively in agreement with the fact that extreme experimental conditions are needed to achieve nitride formation.

Table 9. Gibbs free energies for Equations (3) and (4) for Dy and Sm [kcal mol^{-1}].

Reaction		25 °C	300 °C
3	Sm	84.00	63.80
	Dy	96.71	75.70
4	Sm	67.54	40.76
	Dy	75.73	33.09

Conclusions

The reaction of [Cp_3Ln] complexes with liquid ammonia (Ln = Sm, Gd, Dy, Ho, Er, Yb) yielded sublimable ammine complexes. Other lanthanide metallocenes (Ce, Nd, Eu) also reacted with NH_3, but did not show thermal stability. Structural analysis, carried out for the first time for [Cp_3LnNH_3] compounds, showed that the Ln–N distances do not increase linearly from **1**-Er to **1**-Gd. The Gd complex showed surprisingly long Ln–NH_3 bonds, and structural analysis of **1**-Sm remains problematic, due to the difficulties of crystallisation. Geometry optimisations and calculations of the Gibbs free energies for the ammine products suggested little difference in behaviour. Therefore, intermolecular effects during the solidification process are considered to be responsible for the stabilisation of the NH_3 group for **1**-Sm to **1**-Yb.

Thermal decomposition yielding [{Cp_2LnNH_2}$_2$] (**2**-Ln) occurred for **1**-Yb, **1**-Er, **1**-Ho and **1**-Dy only. In contrast, **1**-Sm and **1**-Gd sublime before the decomposition to the amido complex. X-ray data of amido–cyclopentadienyl–lanthanide(III) complexes were collected for the first time and proved the formation of a dimeric species. DFT calculations performed for the respective monomers showed that decomposition to the amide [Eq. (2)] at higher temperatures changes significantly from **1**-Dy (1.60 kcal mol^{-1}) to **1**-Sm (5.83 kcal mol^{-1}), and confirmed the experimental results.

Further pyrolysis of **1**-Ln and **2**-Ln with inorganic bases [Eq. (3)–(5)] resulted in the formation of reactive nanocrystalline lanthanide nitride powders with an estimated particle size of about 40–90 nm. LiCp was observed as a byproduct and could be separated easily by using organic solvents or sublimation in vacuo. Results of temperature-dependent X-ray powder diffraction experiments proved the formation of LnN at temperatures less than 300 °C. The decomposition of **1**-Ln and **2**-Ln without the use of inorganic bases resulted in the need for higher temperatures for the formation of LnN and higher contamination by graphite, due to the complete decomposition of the Cp ligand.

DFT calculations carried out for the decomposition process of the amido [Eq. (3)] and the ammine [Eq. (4)] complexes in the gas phase showed that the reaction still remains endothermic at 300 °C. Surprisingly, Reaction 4 [Eq. (4)] showed slightly lower endergonic Gibbs free energies than Reaction 3 [Eq. (3)]. These theoretical results could not be verified by the experimental observations made (temperature-dependent X-ray powder diffraction measurements). Thus, no difference between these two reaction pathways was observed. Therefore, advanced solid-state effects seem to be responsible for the fact that nitride material was formed easily at temperatures less than 300 °C. Further investigations on packing effects, base catalysis and intermolecular activation could elucidate the mechanism and reasons for this new convenient pathway to reactive lanthanide nitrides.

Experimental Section

All manipulations described below were performed with rigorous exclusion of oxygen and moisture in flame-dried Schlenk-type glassware on a Schlenk line, interfaced to a vacuum (10^{-3} mbar) line or in an argon-filled glovebox. Argon was purified by passage over columns of silica gel, molecular sieve, KOH, P_4O_{10} and titanium sponge (650 °C), and nitrogen by passage over columns of silica gel, molecular sieve, KOH, P_4O_{10}, BTS[56] and Cr^{II} oxide catalyst.[57] Ammonia was predried by passage over columns of KOH and Cr^{II} oxide catalyst,[57] and then condensed and stored over Na and K before use. THF was predried over KOH and distilled under argon over NaK alloy (benzophenone as indicator). Anhydrous lanthanide(III) chlorides were purchased from Alfa Aesar (99.99 %, ultra dry) and were used as obtained. $LiNH_2$ and CaH_2 were prepared according to the literature.[56] NaCp was prepared according to a novel literature method.[58] [LnCp3] compounds (Ln = Nd, Sm, Eu, Gd, Dy, Ho, Er, Yb) were prepared according to well-known procedures[59] and before use were sublimed twice under vacuum (10^{-3} mbar) at temperatures of between 150 and 250 °C. The syntheses of complexes **1**-Ln and **2**-Ln are based mainly on a procedure reported earlier, in particular for the Yb compounds. Because significant experimental variations were necessary for the syntheses of these compounds, a short protocol containing analytical data for every species is given.

FTIR and FT-Raman spectra were recorded by using a Bruker IFS 66v/S spectrometer with DTGS detector. The samples were thoroughly mixed with dried KBr. The preparation procedures were performed in a glovebox under dried argon atmosphere. The spectra were collected within the range 400 to 4000 cm^{-1} with a resolution of 2 cm^{-1}. During the measurement, the sample chamber was evacuated. For FT-Raman measurements, a Bruker FRA 106/S Raman module with a Nd:YAG laser ($\lambda = 1064$ nm) and a scanning range of 0 to 3500 cm^{-1} was used. Mass spectra were measured by using a JEOL MStation JMS700. The source was operated at a temperature of 200 °C. Temperature-dependent in situ measurements were performed as follows: a Schlenk tube containing the sample was attached directly to the probe chamber of the spectrometer and evacuated until the necessary pressure was reached (10^{-6} mbar). The tube was then fitted in a Carbolite MTF 9/15/130 furnace and heated to 300 °C (5 °C min^{-1}). During the heating phase, EIMS$^+$ spectra were collected in steps of 5 °C. DSC curves from 20 to 800 °C were recorded by using a Metler-Toledo DSC 25, using aluminium crucibles. All measurements were carried out under nitrogen atmosphere. Scanning electron microscopy (SEM) measurements were carried out by using a JEOL JSM-6500F (field emission source). Electron diffraction and microscopy experiments were performed by using a JEOL-JEM 2011 transmission electron microscope (TEM, 200 kV). The powder diffraction investigations were carried out in Debye–Scherrer geometry and diffraction data were collected by using a conventional powder diffractometer (STOE Stadi P, Mo and $Cu_{K\alpha 1}$ radiation). Temperature-dependent measurements were performed by using the same diffractometer ($Mo_{K\alpha 1}$ radiation) with a STOE furnace: Samples were enclosed in silica capillaries and heated from RT up to 900 °C and investigated within the angular range $4.5° \leq 2\theta \leq 20.5°$. Powder diffraction patterns were recorded mostly in temperature steps of 20 K. Products were identified by using the STOE WinXPOW program package (Version 1.22, 1999).

General procedure for [Cp_3LnNH_3] (Ln = Sm (1-Sm), Gd (1-Gd), Dy (1-Dy), Ho (1-Ho), Er (1-Er), Yb (1-Yb)): Anhydrous ammonia was condensed at −78 °C (dry ice, *i*PrOH) onto [$LnCp_3$] (4–10 mmol). The resulting colourless mixture was stirred rapidly for 1–10 h and then allowed to stir for an additional 6–24 h without further cooling. After complete evaporation of residual ammonia, the pale-coloured solid was dried under vacuum (10^{-2}–10^{-3} mbar, RT), removed from the glass wall of the Schlenk tube, recollected at the bottom of the Schlenk and sublimed under reduced pressure (10^{-2}–10^{-3} mbar, 180–210 °C). The sublimation yielded crystalline **1**-Ln (50–91 %). Suitable single crystals were obtained directly from the glass wall of the Schlenk tube or after subsequent sublimation.

1-Sm: [Cp_3Sm] (3.40 g, 9.8 mmol); 30 mL NH_3; stirring time 1 h at −78 °C, 10 h without further cooling; subl. temp. 180 °C; yield 2.98 g

(81%), yellow/orange crystals. IR (KBr): $\tilde{\nu}$ = 3535 (w), 3365 (m), 3322 (s), 3252 (ss), 3188 (m), 3165 (m), 3086 (m), 2707 (w), 2415 (w), 1732 (wbr), 1651 (mbr), 1600 (ss), 1439 (ms), 1356 (m), 1230 (s), 1216 (s), 1124 (w), 1058 (m), 1010 (ss), 874 (w), 842 (w), 773 (vs), 620 (w), 499 cm^{-1} (mbr); elemental analysis calcd (%) for $C_{15}H_{18}NSm$ (362.7): C 49.7, H 5.0, N 3.9, Sm 41.5; found: C 48.9, H 4.7, N 3.5, Sm 42.0.

1-Gd: [Cp_3Gd] (2.30 g, 6.5 mmol); 25 mL NH_3; stirring time 2 h at −78 °C, 24 h without further cooling; subl. temp. 190 °C; yield 1.83 g (76%), colourless crystals. IR (KBr): $\tilde{\nu}$ = 3914 (w), 3323 (m), 3254 (m), 3191 (vw), 3167 (w), 1961 (vw), 2711 (vw), 2418 (vw), 1765 (vw), 1602 (m), 1436 (w), 1358 (w), 1238 (m), 1125 (vw), 1059 (vw), 1009 (m), 877 (w), 844 (w), 775 (s), 666 (w), 622 (w), 535 cm^{-1} (w); elemental analysis calcd (%) for $C_{15}H_{18}NGd$ (369.6): C 48.7, H 4.9, N 3.8, Gd 42.5; found: C 47.5, H 4.7, N 3.4, Gd 42.7.

1-Dy: [Cp_3Dy] (2.07 g, 5.8 mmol); 30 mL NH_3; stirring time 2 h at −78 °C, 14 h without further cooling; subl. temp. 210 °C; yield 1.09 g (50%), pale-yellow crystals. IR (KBr): $\tilde{\nu}$ = 3916 (w), 3571 (vw), 3368 (w), 3324 (m), 3258 (s), 3191 (w), 3168 (w), 3080 (w), 3069 (w), 2712 (vw), 2418 (vw), 1766 (w), 1649 (w), 1602 (s), 1441 (w), 1436 (w), 1358 (vw), 1226 (s), 1126 (vw), 1060 (w), 1010 (s), 878 (w), 843 (w), 776 (s), 668 (w), 621 (w), 511 cm^{-1} (m); MS (70 eV): *m*/*z* (%): 359 (11) [$DyCp_3^+$], 294 (36) [DyC_2^+], 229 (10) [$DyCp^+$], 164 (4) [Dy^+], 66 (100) [$C_5H_6^+$], 65 (40) [$C_5H_5^+$], 39 (33) [$C_3H_3^+$], 17 (5) [NH_3^+].

1-Ho: [Cp_3Ho] (2.49 g, 6.9 mmol); 30 mL NH_3; stirring time 2 h at −78 °C, 12 h without further cooling; subl. temp. 180 °C; yield 2.17 g (83%), orange crystals. IR (KBr): $\tilde{\nu}$ = 3917 (w), 3859 (w), 3322 (s), 3254 (s), 3194 (w), 3169 (m), 3091 (m), 2714 (w), 2421 (vw), 1768 (m), 1650 (m), 1603 (s), 1436 (m), 1358 (m), 1244 (vs), 1060 (m), 1008 (vs), 880 (m), 845 (sh), 775 (vs), 621 (w), 525 cm^{-1} (m); elemental analysis calcd (%) for $C_{15}H_{18}NHo$ (377.3): C 47.8, H 4.8, N 3.7, Ho 43.7; found: C 48.5, H 4.7, N 3.0, Ho 44.4.

1-Er: [Cp_3Er] (3.17 g, 8.7 mmol); 30 mL NH_3; stirring time 6 h at −78 °C, 10 h without further cooling; subl. temp. 200 °C; yield 3.01 g (91%), pink crystals. IR (KBr): $\tilde{\nu}$ = 3552 (m), 3366 (w), 3331 (s), 3300 (w), 3258 (ss), 3193 (w), 3170 (w), 3090 (m), 2708 (w), 2417 (w), 1768 (wb), 1650 (wb), 1603 (s), 1548 (m), 1437 (ms), 1358 (m), 1232 (s), 1122 (w), 1060 (w), 1010 (ss), 891 (w), 844 (w), 701 (vs), 690 (m), 525 (w), 469 (w), 451 (w), 432 cm^{-1} (w); elemental analysis calcd (%) for $C_{15}H_{18}NEr$ (379.6): C 47.5, H 4.8, N 3.7, Er 44.1; found: C 46.4, H 4.1, N 3.7, Er 43.8.

1-Yb: [Cp_3Yb] (1.51 g, 4.1 mmol); 30 mL NH_3; stirring time 2 h at −78 °C, 14 h without further cooling; subl. temp. 180 °C; yield 1.41 g (89%), green crystals. IR (KBr): $\tilde{\nu}$ = 3558 (mb), 3368 (w), 3333 (s), 3261 (ss), 3171 (w), 3092 (w), 2715 (w), 2421 (w), 1772 (wbr), 1661 (wbr), 1603 (s), 1442 (m), 1365 (w), 1232 (s), 1121 (w), 1060 (w), 1012 (ss), 891 (w), 781 (vs), 669 (w), 523 cm^{-1} (w); elemental analysis calcd (%) for $C_{15}H_{18}NYb$ (385.4): C 46.7, H 4.7, N 3.6, Yb 44.9; found: C 46.0, H 4.0, N 3.3, Yb 45.0.

General procedure for [{Cp_2LnNH_2}$_2$] (Ln = Dy (2-Dy), Ho (2-Ho), Er (2-Er), Yb (2-Yb)): A Schlenk tube was flame dried, set under nitrogen atmosphere and filled with [Cp_3DyNH_3] (500 mg, 1.33 mmol). The Schlenk tube was heated (200–290 °C) under slight argon or nitrogen overpressure (30–85 mbar). Formation of both a colourless amorphous and a crystalline solid were observed after sublimation (200–250 °C). Isolation of the crystalline part of the sublimate and further analysis proved the formation of **2**-Ln (17–70%). Single crystals were obtained directly from the glass wall of the Schlenk reaction tube.

2-Dy: [Cp_3DyNH_3] (500 mg, 1.3 mmol); reaction temperature 290 °C; subl. temp. 250 °C; yield 70.8 mg (17%), colourless crystals. IR (KBr): $\tilde{\nu}$ = 3546 (w), 3345 (vw), 3293 (w), 3074 (w), 2703 (vw), 1742 (vw), 1638 (vw), 1539 (w), 1436 (vw), 1353 (vw), 1310 (vw), 1121 (vw), 1061 (vw), 1010 (m), 885 (vw), 845 (vw), 781 (s), 762 (s), 667 (m), 438 cm^{-1} (w); MS (70 eV): *m*/*z* (%): 617 (16) [M^+], 552 (98) [$Dy_2Cp_3N_2H_4^+$], 535 (40) [$Dy_2Cp_3NH_2^+$], 516 (10) [$Dy_2Cp_3^+$], 486 (3) [$Dy_2Cp_2NH_2^+$], 469 (13) [$Dy_2Cp_2N^+$], 403 (9) [Dy_2CpN^+], 359 (22) [$DyCp_3^+$], 294 (100) [$DyCp_2^+$], 229 (26) [$DyCp^+$], 164 (6) [Dy^+], 66 (52) [$C_5H_6^+$], 65 (23) [$C_5H_5^+$], 39 (13) [$C_3H_3^+$], 17 (2) [NH_3^+].

2-Ho: [Cp_3HoNH_3] (1.86 g, 4.9 mmol); reaction temperature 240 °C; subl. temp. 210 °C; yield 1.08 g (70%), pale-pink crystals. IR (KBr): $\tilde{\nu}$ = 3915 (vw), 3549 (m), 3347 (vw), 3296 (w), 3075 (w), 2704 (vw), 1744 (vw), 1639 (w), 1542 (m), 1436 (w), 1322 (w), 1121 (vw), 1061 (vw), 1010 (s), 886 (vw), 782 (vs), 764 (s), 673 (s), 444 cm^{-1} (m); MS (70 eV): *m*/*z* (%): 622 (2) [M^+], 557 (16) [$Ho_2Cp_3N_2H_4^+$], 540 (6) [$Ho_2Cp_3NH^+$], 474 (2) [$Ho_2Cp_2N^+$], 360 (8) [$HoCp_3^+$], 295 (32) [$HoCp_2^+$], 230 (6) [$HoCp^+$], 165 (2) [Ho^+], 66 (100) [$C_5H_6^+$], 65 (40) [$C_5H_5^+$].

2-Er: [Cp_3ErNH_3] (2.65 g, 7.0 mmol); reaction temperature 250 °C; subl. temp. 220 °C; yield 1.40 g (65%), pink crystals. IR (KBr): $\tilde{\nu}$ = 3553 (m), 3365 (w), 3350 (w), 3300 (s), 3087 (m), 2706 (w), 2413 (w), 2271 (w), 1747 (wb), 1642 (wb), 1548 (s), 1437 (ms), 1354 (m), 1258 (w), 1232 (w), 1121 (w), 1060 (w), 1010 (ss), 886 (w), 844 (w), 783 (vs), 765 (vs), 683 (s), 451 cm^{-1} (w); elemental analysis calcd (%) for $C_{10}H_{12}NEr$ (313.47): C 38.3, H 3.9, N 4.5, Er 53.3; found: C 36.9, H 4.0, N 4.1, Er 53.6.

2-Yb: [Cp_3YbNH_3] (765 mg, 2.0 mmol); reaction temperature 250 °C; subl. temp. 220 °C; yield 494 mg (78%), yellow crystals. IR (KBr): $\tilde{\nu}$ = 3562 (m), 3545 (w), 3304 (s), 3097 (m), 2707 (w), 2410 (w), 1753 (wbr), 1640 (wbr), 1558 (s), 1438 (ms), 1370 (m), 1121 (w), 1060 (w), 1010 (ss), 891 (w), 784 (vs), 767 (vs), 703 (s), 510 cm^{-1} (w).

Procedures for the pyrolysis reaction to LnN (Ln = Sm, Gd, Dy, Ho, Er, Yb)

Route A ([Eq. (3)], Ln = Ho, Er, Yb): **2**-Ln (0.5–1.5 mmol) was mixed together with $LiNH_2$ (1.5–3.0 mmol), ground thoroughly in a mortar and transferred to a glazed clay crucible situated in a quartz tube, which was connected to a Schlenk line. The boat was heated to 188 °C (2 °C min^{-1}) under argon atmosphere. After 6 d at this temperature, the tube was cooled to RT and the brown powder was analysed by X-ray powder diffraction (XRD). After opening the tube under argon atmosphere, the typical smell of ammonia was detected. Subsequently, the mixture was heated to 250 °C (2 °C min^{-1}) for 3 d and then cooled to RT. The formation of a colourless, feltlike crystalline solid covering the brown solid in the crucible was observed. Again, after opening the tube under argon atmosphere, the typical smell of ammonia was detected. Subsequently, the solid was thoroughly ground in a mortar and heated to 250 °C under vacuum (10^{-3} mbar) for a further 2 d. The formation of a colourless microcrystalline powder was observed at the cooler part of the tube and a dark brown solid remained inside the alumina boat. The brown solid was identified by X-ray powder diffractometry as erbium nitride. Elemental analysis calcd (%) for ErN (181.3): C 0.0, H 0.0, N 7.7, Er 92.1; found: C 1.5, H 0.1, N 7.9, Er 90.8.

Route B ([Eq. (4)], Ln = Dy, Ho, Er): **1**-Ln (0.3–1.0 mmol) was mixed together thoroughly with (0.9–3.0 mmol) of $LiNH_2$ in an alumina crucible situated inside a quartz tube, which was connected to a Schlenk line and heated to 200 °C (2 °C min^{-1}) under nitrogen or argon atmosphere. After 24 h at this temperature, the following procedure was repeated three times: the tube was heated to 260 °C (2 °C min^{-1}) for 12 h and afterwards cooled to RT (4 °C min^{-1}). To achieve complete reaction of the components the crude product was ground thoroughly in a mortar.

Formation of a colourless crystalline solid was observed at the cooler part of the tube after heating. Opening of the tube under argon atmosphere revealed the typical smell of ammonia and on the top of the crucible, the formation of a colourless feltlike film over the crude product was observed. Both products were identified by X-ray powder diffractometry as cyclopentadienyl–lithium[55] and lanthanide nitride. CpLi: IR (KBr): $\tilde{\nu}$ = 3938 (w), 3677 (w), 3087 (w), 2922 (w), 2677 (w), 2396 (w), 2023 (w), 1757 (w), 1642 (m), 1544 (m), 1433 (w), 1259 (w), 1005 (m), 748 (s), 520 cm^{-1} (m); elemental analysis calcd (%) for ErN (181.3): C 0.0, H 0.0, N 7.9, Er 92.1; found: C 3.2, H 0.2, N 8.3, Er 87.9.

Route C ([Eq. (5)]): **2**-Yb (493 mg, 1.54 mmol) was mixed together with CaH_2 (130 mg, 3.1 mmol) in a glazed clay crucible situated inside a quartz tube, which was connected to a Schlenk line and then heated to 360 °C (1 °C min^{-1}) under argon atmosphere. After 7 d at this temperature, the tube was cooled to RT (1 °C min^{-1}). The formation of small amounts of colourless, green, orange, yellow and red crystals was observed at the cooler part of the tube. After opening the tube under argon atmosphere, the typical smell of ammonia was detected and inside the crucible, a black microcrystalline solid was formed. The black solid was

identified by X-ray powder diffractometry as ytterbium nitride. The side products were identified by single-crystal diffractometry as $[Cp_3Yb]$, $[CaCp_2]$ and $[Yb_xCa_{1-x}Cp_2]$.

X-ray single-crystal data collection, structure solution and refinement

Because reflection data were collected by using different instruments, data reduction was performed by using different program packages and will be reported for each crystal. In the discussion of data of higher quality, only the low-temperature measurements will be mentioned in this article. Nevertheless, both low-temperature and RT data are available at CCDC. CCDC 287096–287111 contain the supplementary crystallographic data for this paper. These data can be obtained free of charge from The Cambridge Crystallographic Data Centre via www.ccdc.cam.ac.uk/data_request/cif. Subsequent calculations after the determination of the unit-cell parameters and data reduction to the hkl-format were carried out by using the SHELXS[60] and SHELXL[61] programs. The analytical scattering factors for neutral atoms were used throughout the analysis. Hydrogen atoms were either treated isotropically, if found in the Fourier maps, or were included manually by using a riding model.

*$[Cp_3GdNH_3]$ (**1**-Gd)*: The diffraction symmetry was $m\bar{3}$ and the systematic absences were consistent with the centrosymmetric cubic space group $Pa\bar{3}$, which was later determined to be correct. The structure of **1**-Gd was solved by direct methods and refined on F^2 by using full-matrix least-square techniques. The Ln–N bond is located along the 3-fold axis of the unit cell, so that only a C_5H_5GdNH fragment is situated in the asymmetric unit and the metal atom and the nitrogen atom are located on special positions. The STOE IPDS program package was used to determine the unit-cell parameters, for data collection and to transform the raw data into the reflection-data file. The refinement was carried out by using unmerged data to obtain more precise results. Further details are given in Table 1, and bond lengths and angles are listed in Table 2.

*$[Cp_3LnNH_3]$ (**1**-Dy, **1**-Ho, **1**-Er)*: The diffraction symmetry was $2/m$ and the systematic absences were consistent with the centrosymmetric monoclinic space group $P2_1/c$, which was later determined to be correct. The structures of **1**-Dy, **1**-Ho and **1**-Er were solved by direct methods and refined on F^2 by using full-matrix least-square techniques. The STOE IPDS program package was used for **1**-Ho to determine the unit-cell parameters, for data collection and to transform the raw data into the reflection-data file. However, for **1**-Dy and **1**-Er the Collect program package (scalepack cell, hkl scalepack and hkl Denzo) was used to determine the unit-cell parameters, for data collection and to transform the raw data into the reflection-data file. Further details are given in Table 1, and bond lengths and angles are listed in Table 2.

*$[\{Cp_2LnNH_2\}_2]$ (**2**-Dy, **2**-Ho and **2**-Yb)*: The diffraction symmetry was $2/m$ and the systematic absences were consistent with the centrosymmetric monoclinic space group $P2_1/n$, which was later determined to be correct. The structures of **2**-Dy, **2**-Ho and **2**-Yb were solved by direct methods and refined on F^2 by using full-matrix least-square techniques. A 2-fold axis is situated in the centre of the dimeric complex, therefore, only one half of the entire molecule is situated in the asymmetrical unit. The STOE IPDS program package was used to determine the unit-cell parameters, for data collection and to transform the raw data into the reflection-data file. Further details are given in Table 5, and bond lengths and angles are listed in Table 6.

*$[\{Cp_2ErNH_2\}]_2]$ (**2**-Er)*: The diffraction symmetry was $m\bar{3}$ and the systematic absences were consistent with the centrosymmetric cubic space group $Im\bar{3}$, which was later determined to be correct. The structure of **2**-Er was solved by direct methods and refined on F^2 by using full-matrix least-square techniques. The molecular structure is highly symmetrical, so that three carbon, four hydrogen, one nitrogen and one erbium atom are situated in the asymmetrical unit of the elementary cell. The Collect program package (scalepack cell, hkl scalepack and hkl Denzo) was used to determine the unit-cell parameters, for data collection and to transform the raw data into the reflection-data file. The refinement was carried out by using unmerged data to obtain more precise results. Further details are given in Table 5, and bond lengths and angles are listed in Table 6.

Acknowledgements

The authors are indebted to the following people for conducting the physical measurements: Dr. Oliver Oeckler and Dr. Peter Mayer (single-crystal X-ray diffractometry), Dr. Markus Döblinger (TEM experiments), Dagmar Ewald and Dr. Gerd Fischer (mass spectrometry), Sascha Correll (temperature-dependent X-ray powder diffractometry) and Dr. Sabine Beyer (differential scanning calorimetry) (all Department Chemie und Biochemie, Universität München (LMU)). Financial support from the Deutsche Forschungsgemeinschaft (DFG) (Schwerpunktprogramm SPP 1166, Lanthanoidspezifische Funktionalitäten in Molekül und Material, project SCHN377/10) and the Fonds der Chemischen Industrie is also gratefully acknowledged. Laurent Maron and Noémi Barros are grateful to CINES and CALMIP for being granted computing time.

[1] L. Abis, D. Belli Dell'Amico, C. Busetto, F. Calderazzo, R. Caminiti, C. Ciofi, F. Garbassi, G. Masciarelli, *J. Mater. Chem.* **1998**, *8*, 751–759.
[2] L. Abis, D. Belli Dell'Amico, C. Busetto, F. Calderazzo, R. Caminiti, F. Garbassi, A. Tomei, *J. Mater. Chem.* **1998**, *8*, 2855–2861.
[3] Y. K. Gun'ko, F. T. Edelmann, *Comments Inorg. Chem.* **1997**, *19*, 153–184.
[4] L. G. Hubert-Pfalzgraf, *New J. Chem.* **1995**, *19*, 727–750.
[5] J. W. Stouwdam, F. C. J. M. v. Veggel, *ChemPhysChem* **2004**, *5*, 743–746.
[6] M. Veith, S. Mathur, H. Shen, N. Lecerf, S. Hüfner, M. H. Jilavi, *Chem. Mater.* **2001**, *13*, 4041–4052.
[7] A. Weber, H. Suhr, H. Schumann, R.-D. Köhn, *Appl. Phys. A* **1990**, *51*, 520–525.
[8] D. Hanaoka, S. Ito (Sharp Corp., Japan), JP 2001148540, **2001**; [*Chem. Abstr.* **2001**, *134*, 373859].
[9] M. Martens, *Ingenieursblad* **1971**, *40*, 287–291.
[10] H. Tanaka, M. Hashimoto, S. Emura, A. Yanase, R. Asano, Y. K. Zhou, H. Bang, K. Akimoto, T. Honma, N. Umesaki, H. Asahi, *Phys. Status Solidi C* **2003**, *0*, 2864–2868.
[11] T. C. Kirk, E. G. Lundquist, T. R. Lynn (Rohm & Haas, USA), EP 1367070, **2003**; [*Chem. Abstr.* **2003**, *139*, 396303].
[12] G. A. Molander, J. A. C. Romero, *Chem. Rev.* **2002**, *102*, 2161–2185.
[13] R. E. Murray (Union Carbide Chem. Plastic, USA), WO 9901460, **1999**; [*Chem. Abstr.* **1999**, *130*, 125530].
[14] T. Juestel, P. Schmidt, H. Höppe, W. Schnick, W. Mayr (Philips Intellectual Property & Standards GmbH, Germany; Koninklijke Philips Electronics N. V.; Lumileds Lighting U. S. Llc), WO 2004055910, **2004**; [*Chem. Abstr.* **2004**, *141*, 96377].
[15] R. Mueller-Mach, G. Mueller, M. R. Krames, H. A. Höppe, F. Stadler, W. Schnick, T. Juestel, P. Schmidt, *Phys. Status Solidi A* **2005**, *202*, 1727–1732.
[16] R. L. LaDuca, P. T. Wolczanski, *Inorg. Chem.* **1992**, *31*, 1311–1313.
[17] J. C. Fitzmaurice, A. Hector, A. T. Rowley, I. P. Parkin, *Polyhedron* **1994**, *13*, 235–240.
[18] J. C. Fitzmaurice, A. L. Hector, I. P. Parkin, *J. Chem. Soc. Dalton Trans.* **1993**, 2435–2438.
[19] B. Jürgens, H. A. Höppe, E. Irran, W. Schnick, *Inorg. Chem.* **2002**, *41*, 4849–4851.
[20] B. Jürgens, E. Irran, W. Schnick, *J. Solid State Chem.* **2005**, *178*, 72–78.
[21] B. Jürgens, E. Irran, J. Senker, P. Kroll, H. Müller, W. Schnick, *J. Am. Chem. Soc.* **2003**, *125*, 10288–10300.
[22] P. Kroll, W. Schnick, *Chem. Eur. J.* **2002**, *8*, 3530–3537.
[23] B. V. Lotsch, J. Senker, W. Schnick, *Inorg. Chem.* **2004**, *43*, 895–904.
[24] W. Schnick, *Angew. Chem.* **1999**, *111*, 3511–3512; *Angew. Chem. Int. Ed.* **1999**, *38*, 3309–3310.
[25] W. Schnick, *Int. J. Inorg. Mater.* **2001**, *3*, 1267–1272.
[26] W. Schnick, R. Bettenhausen, B. Götze, H. A. Höppe, H. Huppertz, E. Irran, K. Köllisch, R. Lauterbach, M. Orth, S. Rannabauer, T. Schlieper, B. Schwarze, F. Wester, *Z. Anorg. Allg. Chem.* **2003**, *629*, 902–912.
[27] S. Arndt, J. Okuda, *Chem. Rev.* **2002**, *102*, 1953–1976.

[28] W. J. Evans, J. H. Meadows, A. L. Wayda, W. E. Hunter, J. L. Atwood, *J. Am. Chem. Soc.* **1982**, *104*, 2008–2014.
[29] M. A. Giardello, V. P. Conticello, L. Brard, M. Sabat, A. L. Rheingold, C. L. Stern, T. J. Marks, *J. Am. Chem. Soc.* **1994**, *116*, 10212–10240.
[30] J. M. Birmingham, G. Wilkinson, *J. Am. Chem. Soc.* **1956**, *78*, 42–44.
[31] E. O. Fischer, H. Fischer, *J. Organomet. Chem.* **1966**, *6*, 141–148.
[32] H. Fischer, *PhD thesis*, Technische Hochschule München, Germany, **1965**.
[33] R. D. Fischer, H. Fischer, *J. Organomet. Chem.* **1965**, *4*, 412–414.
[34] F. Calderazzo, R. Pappalardo, S. Losi, *J. Inorg. Nucl. Chem.* **1965**, *28*, 987–999.
[35] J. Müller, *Chem. Ber.* **1969**, *102*, 152–160.
[36] R. G. Hayes, J. L. Thomas, *Inorg. Chem.* **1969**, *8* 2521–2522.
[37] L. Maron, O. Eisenstein, *J. Phys. Chem. A* **2000**, *104*, 7140–7143.
[38] M. Dolg, O. Fulde, W. Küchle, C.-S. Neumann, H. Stoll, *J. Chem. Phys.* **1991**, *94*, 3011–3017.
[39] M. Dolg, H. Stoll, H. Preuss, *Theor. Chim. Acta* **1993**, *85*, 441–450.
[40] M. Dolg, H. Stoll, A. Savin, H. Preuss, *Theor. Chim. Acta* **1989**, *75*, 173–194.
[41] A. D. Becke, *J. Chem. Phys.* **1993**, *98*, 5648–5652.
[42] K. Burke, J. P. Perdew, W. Yang in *Electronic Density Functional Theory: Recent Progress and New Directions*, 1st ed. (Eds.: J. F. Dobson, G. Vignale, M. P. Das), Plenum, New York, **1998**.
[43] E. Folga, T. Ziegler, L. Fan, *New J. Chem.* **1991**, *15*, 741–748.
[44] L. Maron, O. Eisenstein, *J. Am. Chem. Soc.* **2001**, *123*, 1036–1039.
[45] H. Rabaa, J.-Y. Saillard, R. Hoffmann, *J. Am. Chem. Soc.* **1986**, *108*, 4327–4333.
[46] E. C. Sherer, C. J. Cramer, *Organometallics* **2003**, *22*, 1682–1689.
[47] M. J. Frisch, G. W. Trucks, H. B. Schlegel, G. E. Scuseria, M. A. Robb, J. R. Cheeseman, V. G. Zakrzewski, J. A. Montgomery, R. E. Stratman, J. C. Burant, S. Dapprich, J. M. Millam, A. D. Daniels, K. N. Kudin, M. C. Strain, O. Farkas, J. Tomasi, V. Barone, M. Cossi, R. Cammi, B. Mennucci, C. Pomelli, C. Adamo, S. Clifford, J. Ochterski, G. A. Petersson, P. Y. Ayala, P. Y. Cui, K. Morokuma, D. K. Malick, A. D. Rabuck, K. Raghavachari, J. B. Foresman, J. Cioslowski, J. V. Ortiz, B. B. Stefanov, G. Liu, A. Liashenko, P. Piskorz, I. Komaromi, G. Gomperts, R. L. Martin, D. J. Fox, T. Keith, M. A. Al-Laham, C. Y. Peng, A. Nanayakkara, C. Gonzalez, M. Challacombe, P. M. W. Gill, B. G. Johnson, W. Chen, M. W. Wong, J. L. Andres, M. Head-Gordon, E. S. Replogle, J. A. Pople *Gaussian 98 (Revision A.9)*, Gaussian, Inc., Pittsburgh PA (USA), **1998**.
[48] "Lanthanide and Actinide Chemistry and Spectroscopy": R. D. Fischer, G. Bielang, *ACS Symp. Ser.* **1980**, *4*, 60–79.
[49] R. Anwander, W. A. Herrmann, *Top. Curr. Chem.* **1996**, *179*, 1–33.
[50] S. Manastyrskyj, R. E. Maginn, M. Dubeck, *Inorg. Chem.* **1963**, *2*, 904–905.
[51] W. Lamberts, H. Lueken, *Inorg. Chim. Acta* **1987**, *132*, 119–122.
[52] W. Lamberts, H. Lueken, B. Hessner, *Inorg. Chim. Acta* **1987**, *134*, 155–157.
[53] H. Lueken, J. Schmitz, W. Lamberts, P. Hannibal, K. Handrick, *Inorg. Chim. Acta* **1989**, *156*, 119–124.
[54] Z. Wu, Z. Xu, X. You, H. Wang, *Polyhedron* **1993**, *12*, 677–681.
[55] R. E. Dinnebier, U. Behrens, F. Olbrich, *Organometallics* **1997**, *16*, 3855–3858.
[56] G. Brauer in *Handbuch der Präparativen Anorganischen Chemie, Vol. 1*, 3rd ed. (Ed.: G. Brauer), Ferdinand Enke, Stuttgart, **1975**, pp. 444–445.
[57] H. L. Krauss, H. Stach, *Z. Anorg. Allg. Chem.* **1969**, *366*, 34–42.
[58] T. K. Panda, M. T. Gamer, P. W. Roesky, *Organometallics* **2003**, *22*, 877–878.
[59] F. T. Edelmann in *Lanthanides and Actinides, Vol. 6*, 1st ed. (Ed.: W. A. Herrmann), Georg Thieme, Stuttgart, New York, **1997**, pp. 88–90.
[60] G. M. Sheldrick *SHELXS-97*, University of Göttingen, Göttingen, **1997**.
[61] G. M. Sheldrick *SHELXL-97*, University of Göttingen, Göttingen, **1997**.

Received: October 23, 2005
Published online: March 10, 2006

